Journal of Solid State Chemistry **168,** 284–293 (2002)
doi:10.1006/jssc.2002.9723

Effects of Pressure and Temperature on the Formation of Tungsten-Bronze-Related Phases, RE_xWO_{3+y}, with RE = La and Nd

C. Grenthe,* M. Sundberg,*,[1] V. P. Filonenko,† and I. P. Zibrov‡

*Department of Inorganic Chemistry, Arrhenius Laboratory, Stockholm University, S-106 91 Stockholm, Sweden; †Institute for High Pressure Physics, Russian Academy of Sciences, Troitsk, 142190 Moscow Region, Russia; and ‡Institute of Crystallography, Russian Academy of Sciences, 117 333 Moscow, Russia

Received April 22, 2002; in revised form July 2, 2002; accepted July 16, 2002

The influence of pressure (P) and temperature (T) on the formation of tungsten-bronze-related phases containing lanthanum and neodymium was investigated. A large number of samples with bulk compositions RE_xWO_3, prepared by solid-state reaction in the pressure and temperature regions P = 10–80 kbar and T = 1170–1620 K were examined by X-ray powder diffraction and electron microscopy, and a (P–T) diagram showing the phase relations was drawn. Three tungsten-bronze-related phases with perovskite (PTB)-, hexagonal (HTB)- and intergrowth (ITB)-type structures were identified. The PTB bronze RE_xWO_3 with $x \approx 0.10$ was formed at $p \leq 50$ kbar. The HTB-related phase with $x \approx 0.10$ was observed in samples prepared at $P \geq 20$ kbar, whereas phases of (n)-ITB-type were observed only in the 25–50 kbar region. In the latter pressure region, the PTB and ITB phases were only seen in samples prepared at $T > 1520$ K, while the HTB-related phase was found in almost all samples. The HTB- and ITB-related compounds are metastable, probably fully oxidized, high-pressure phases of composition $RE_xWO_{3+3x/2}$ with $x \leq 0.13$. They transform to a cubic PTB bronze during annealing in inert atmosphere under ambient pressure conditions. According to microanalysis studies of individual crystals, less than 40% of the hexagonal tunnel sites in the HTB and ITB structures are occupied by RE^{3+} ions. A superstructure of HTB-type with $\approx$60% occupancy of the hexagonal tunnel sites ($x \approx 0.20$) was observed in a few crystals from the samples prepared at P = 80 kbar. Ordered, defect and intergrowth structures are presented. © 2002 Elsevier Science (USA)

Key Words: **rare-earth tungsten oxides; RE_xWO_{3+y}; high-pressure synthesis; perovskite tungsten bronze; hexagonal tungsten bronze; intergrowth tungsten bronze; X-ray diffraction; electron microscopy; EDS; phase transformation.**

INTRODUCTION

During the last few years, we have studied the WO_3–$RE_2W_2O_9$–WO_2 part of WO_3–RE_2O_3–W systems with RE = La, Pr and Nd, seeking to establish possible relationships between structural chemistry and synthesis conditions. Preparations have been carried out at high pressure, using a chamber of toroid type (1–4), and at ambient pressure conditions by conventional solid-state synthesis in air or in evacuated silica tubes (5, 6). X-ray powder diffraction, high-resolution transmission electron microscopy (HRTEM), energy-dispersive X-ray spectroscopy (EDS) and thermal analysis methods have been used for characterization of the materials.

The first two high-pressure experiments were made in the systems Nd_2O_3–WO_3 (1) and Pr_2O_3–WO_3 (2) at P = 50 kbar. HRTEM studies revealed that multiphase samples containing several new phases had been produced. Crystals with structures of hexagonal tungsten bronze (HTB) and intergrowth tungsten bronze (ITB) types were identified from HRTEM images. The latter structures were the members n = 2, 3 and 4 of the (n)-ITB family of related phases. Previous X-ray studies of rare-earth tungsten oxide samples, prepared by conventional solid-state synthesis under ambient pressure conditions, have established that $RE_{\sim 0.1}WO_3$ bronzes with structures of perovskite tungsten bronze (PTB) type are formed with RE = La–Lu (7–9).

Recent X-ray powder diffraction and electron microscopy studies of a few RE_xWO_3 samples with RE = La or Nd, x = 0.1 or 0.2, prepared at P = 25–30 kbar and T = 1320–1620 K, showed that RE bronzes with HTB-, PTB- and (n)-ITB-related structures were formed (3, 4). Refinement of the HTB structure of $La_{\sim 0.1}WO_3$ by the Rietveld method suggested that the lanthanum ions are located in the six-sided tunnels close to the tungsten atom plane (4). Thermogravimetric studies of $La_{0.1}WO_3$ samples

[1] To whom correspondence should be addressed. Fax: +46 8 15 21 87. E-mail: marsu@inor.su.se.

0022-4596/02 $35.00

in argon and oxygen atmosphere indicated that additional oxygen ions are present in the hexagonal tunnels, thus forming an almost fully oxidized HTB-related phase of composition $La_{0.1}WO_{3+y}$ with $y \approx 0.15$.

The structural differences between tungsten-bronze-related phases formed under high- and ambient-pressure conditions suggest that additional investigations of RE_xWO_3 samples prepared at different pressures and temperatures are required in order to explore the effects of pressure and temperature on the formation and stability of the RE_xWO_{3+y} phases. The present paper deals with the pressure–temperature phase relationships in the systems WO_3–$RE_2W_2O_9$–WO_2 with RE = La and Nd. A tentative pressure–temperature phase diagram has been drawn, based on a number of La_xWO_3 and Nd_xWO_3 samples prepared in the region P = 10–80 kbar, T = 1170–1620 K.

EXPERIMENTAL

La_xWO_3 and Nd_xWO_3 samples with $0.10 \leq x \leq 0.33$ were synthesized from stoichiometric mixtures of La_2O_3, Nd_2O_3, WO_3 and W metal powder by solid-state reaction in a high-pressure chamber of toroid type, as described by Zibrov *et al.* (10). The resulting mixtures were pressed into pellets, which were wrapped up into tungsten foil to avoid chemical reaction between the sample and the surrounding

TABLE 1
Sample Composition, Synthesis Conditions, Unit-Cell Parameters Refined from the X-Ray Data, Unit-Cell Volume and EDS Results from TEM and SEM Studies of Tungsten-Bronze-Related Phases, La_xWO_3

Sample La_xWO_3 x	P (kbar)	T (K)	Phase	Unit cell dimensions (XRD)				EDS results	
				a (Å)	b (Å)	c (Å)	V (Å^3)	x-Range	Mean
(a) 0.10	80	1620	HTB $W_3O_8^{ED}$ 1:1^{ED} WO_3^{XRD}	7.4063(4)		3.7946(3)	180.26	0.08–0.12,	0.10
(b) 0.10	80	1470	HTB 2xHTB^{ED} $W_3O_8^{ED}$	7.4037(4) 2 × 7.4		3.7951(3) 3.8	180.15	0.09–0.12, 0.2–0.22	0.10
(c) 0.10	50	1620	HTB WO_2^{XRD} WO_3^{XRD}	7.4099(4)		3.7938(3)	180.40	0.06–0.11,	0.08
(d) 0.10	50	1570	HTB WO_3^{XRD}	7.4059(3)		3.7951(3)	180.26	0.08–0.11,	0.09
(e) 0.10	50	1470	HTB 1:1^{ED}	7.4070(5)		3.7936(3)	180.25	0.08–0.12,	0.10
(f) 0.10	30	1620	HTB 2-ITB 3-ITB	7.4045(7) 10.1212(8) 27.738(8)	 7.4037(7) 7.3965(7)	3.7945(4) 3.8151(3) 3.8168(4)	180.16 285.88 783.52	0.10–0.12, 0.07–0.08, 0.04–0.07,	0.11 0.07 0.05
(g) 0.10	30	1320	HTB WO_3^{XRD}	7.4058(3)		3.7929(3)	180.16	0.06–0.12,	0.09
(h) 0.10	25	1520	HTB PTB	7.4089(1) 3.8245(1)		3.7924(1)	180.28 56.94	0.10–0.12, 0.09–0.12,	0.11 0.10
(i) 0.15	25	1520	HTB PTB^{ED} 2–ITB 3–ITB^{ED}	7.4104(6) 3.8 10.1312(11) 27.7	 7.4088(10) 7.4	3.7960(3) 3.8073(6) 3.8	180.53 285.78	0.10–0.12,	0.11

Note. ^{ED}Rare–earth tungsten bronzes and additional phases only observed by ED/EDS, ^{XRD}Additional phases identified from the X-ray powder pattern only.

high-pressure cell material. Most of the La_xWO_3 samples were prepared with the fixed starting composition $x = 0.10$ at the pressures 25, 30, 50 and 80 kbar and at temperatures between 1350 and 1620 K. The composition of the Nd_xWO_3 samples, on the other hand, was varied within the region $0.10 \leq x \leq 0.33$, and most of them were prepared at $P = 10$–80 kbar and 1170–1620 K. The applied pressure was stabilized after approximately 15 min. The sample was then heated to the desired temperature, which was held for 5–20 min and then quenched to room temperature before the pressure was released. The experimental conditions are summarized in Tables 1 and 2.

All samples were analyzed by X-ray powder diffraction, using a Guinier–Hägg focusing camera with monochromatic Cu$K\alpha_1$ radiation and with Si as internal theta standard. The photographs were evaluated with a film scanner (11). The unit-cell dimensions were refined from the X-ray data with the program PIRUM, using least-squares methods (12).

A JEOL 820 scanning electron microscope (SEM), equipped with a LINK AN10000 EDS microanalysis system was used to check the purity of the bulk samples and to determine the *RE*:W ratio. Structural information was obtained from electron diffraction (ED) and microanalysis studies of individual crystals in a JEOL 2000FXII transmission electron microscope, equipped with a LINK AN10000 EDS microanalysis system. The EDS analyses were based on the La*L*, Nd*L* and W*L* peaks in the EDS spectra. Specimens for the transmission electron microscopy (TEM) studies were prepared by crushing small parts of the samples in an agate mortar, dispersing the resulting powders in *n*-butanol and finally putting a few drops of the

TABLE 2
Sample Composition, Synthesis Conditions, Unit-Cell Parameters Refined from the X-Ray Data, Unit-Cell Volume and EDS Results from TEM and SEM Studies of Tungsten-Bronze-Related Phases, Nd_xWO_3

Sample				Unit cell dimensions (XRD)				EDS results	
Nd_xWO_3 x	P (kbar)	T (K)	Phase	a (Å)	b (Å)	c (Å)	V (Å^3)	x-Range	Mean
0.10	80	1470	HTB	7.3872(3)		3.7904(3)	179.13	0.09–0.13,	0.11
			$2 \times$ HTB^{ED}	2×7.4				~0.21	
0.20	80	1520	HTB	7.3875(3)		3.7886(3)	179.06	0.08–0.10,	0.09
			$2 \times$ HTB^{ED}	2×7.4				0.18–0.21,	0.20
			1:1^{ED}						
0.33	80	1520	HTB	7.3891(4)		3.782(6)	178.89	~0.15	
			$2 \times$ HTB^{ED}	2×7.4				0.18–0.20,	0.19
			1:1^{ED}						
			WO_2^{XRD}						
0.10	50	1620	HTB	7.4019(8)		3.7926(5)	179.95	0.07–0.11,	0.09
			PTB	3.8054(4)			55.11		
0.10	30	1570	HTB	7.3906(4)		3.7938(4)	179.46	0.10–0.12,	0.11
			2-ITB	10.093(1)	7.3798(7)	3.8162(6)	284.25	0.07–0.10,	0.08
			3-ITB^{ED}					0.03–0.07,	0.05
			PTB	3.8148(2)			55.52	0.10–0.11,	0.10
0.20	30	1420	HTB	7.3911(2)		3.7914(3)	179.37	0.08–0.14,	0.11
			WO_3^{XRD}						
0.33	30	1320	HTB	7.3860(4)		3.7912(3)	179.12	0.08–0.14,	0.11
			WO_2^{XRD}						
0.10	25	1370	HTB	7.3959(3)		3.7878(2)	179.43	0.07–0.11,	0.09
			PTB	3.8183(3)			55.67		
0.10	25	1170	HTB	7.3906(4)		3.7938(9)	179.45	0.05–0.09,	0.07
			WO_3^{XRD}						
0.15	25	1570	PTB	3.8214(3)			55.81	0.08–0.11,	0.10
0.10	20	1220	HTB	7.389(1)		3.782(1)	178.82	0.08–0.11,	0.10
			PTB	3.811(2)			55.35	0.09–0.11,	0.10
0.10	10	1270	PTB	3.814(2)			55.48	0.08–0.11,	0.10

Note. ^{ED}Rare–earth tungsten bronzes and additional phases only observed by ED/EDS, ^{XRD}Additional phases identified from the X-ray powder pattern only.

suspensions on holey carbon films supported by a copper grid. The HRTEM studies were carried out in a JEOL JEM 3010, operated at an accelerating voltage of 300 kV. The radius of the objective aperture used corresponded to 0.68 $Å^{-1}$ in reciprocal space. Most of the HRTEM images were taken at a defocus value close to the Scherzer condition, so that the dark spots in the images could be interpreted as projected metal atoms. Theoretical images of the structure models were calculated with a locally modified version of the program suite SHRLI (13). The structure models were drawn with the program ATOMS by Shape Software.

RESULTS

The X-ray powder patterns and the electron microscopy studies of about 25–50 crystallites from each La_xWO_3 and Nd_xWO_3 sample showed that multiphase products had been formed. A small amount of WO_3 was observed in some of the samples. About half of the examined crystallites were identified by combination of ED and EDS results from the same region of the crystal fragment. All products were microcrystalline and had a dark-blue color.

X-Ray Diffraction Studies

Several La_xWO_3 samples were synthesized with the same bulk composition ($x = 0.10$) but at different pressures and temperatures. Synthesis conditions, phases identified from X-ray and electron diffraction patterns, unit-cell parameters refined from the X-ray data and EDS results from SEM and TEM studies of individual crystals are all listed in Table 1. Peaks characteristic of an HTB-related phase could be found in all patterns, and the hexagonal unit-cell dimensions were refined from the corresponding X-ray data. The data in Table 1 show that the volume of the hexagonal unit cell is approximately constant, independent of synthesis pressure and temperature, and that the La content in the HTB-type crystals is within the range $x = 0.10 \pm 0.02$. Two of the samples, marked (b) and (e) in Table 1, consisted mainly of the HTB-related phase, whereas sample (h) was composed of two phases, HTB and PTB, in about equal amounts. The X-ray powder pattern of sample (f), prepared at 30 kbar and the highest temperature ($T = 1620$ K), differed from most of the others. All lines in the X-ray pattern could however be identified as belonging to the bronze-related phases (2)-ITB, (3)-ITB and HTB (3). Lines typical of the (2)-ITB phase were also seen in the X-ray pattern from the sample $La_{0.15}WO_3$. Both samples were synthesized at high temperature, $T > 1500$ K.

Lines characteristic of an HTB-related phase could be seen in the X-ray patterns of all Nd samples, regardless of composition, pressure and temperature. The X-ray results in Table 2 show that also here the volume of the HTB cell is approximately constant. The microanalysis results yield an Nd content in the HTB-type crystals within the $x = 0.10 \pm 0.03$ range, as for the La compound. There is an apparent decrease in cell volume when lanthanum is replaced by neodymium in the HTB structure, consistent with the difference in ionic radius between the two elements. The X-ray results in Table 2 also show that a cubic PTB bronze, Nd_xWO_3, was present in all samples with bulk compositions $x \leq 0.15$, prepared below $P = 50$ kbar. Two of these samples prepared at $P \leq 25$ kbar turned out to be monophasic. It is noteworthy that the (2)-ITB phase was only seen in one sample, $Nd_{0.10}WO_3$, prepared at $T = 1570$ K.

Electron Microscopy Studies

The ED pattern in Fig. 1a is typical of an HTB-related phase in [001] projection. Such patterns were taken of several crystals from each sample prepared in the pressure region 20–80 kbar. The reflections were sharp, without any diffuse streaking along the $\langle 100 \rangle$ directions in most of the patterns, thus indicating well-ordered crystals of HTB type.

Superlattice reflections that show a doubled HTB-cell a parameter can be seen in the ED pattern in Fig. 1b. Such patterns were yielded by a few crystals from the samples prepared at the highest pressure, $P = 80$ kbar, especially those with bulk composition $x \geq 0.20$. The EDS analyses indicated an RE content of $x \approx 0.2$, which is about twice that previously observed in the HTB-related crystals.

The HRTEM image in Fig. 1c, with the corresponding ED pattern in Fig. 1a, is taken of a crystallite from the bulk sample $La_{0.10}WO_3$ prepared at $P = 80$ kbar. The contrast features in the image suggest a local variation in the filling of the six-sided tunnels in the HTB structure. The hexagonally arranged dark dots correspond to projected tungsten and lanthanum atoms. The large white spots indicate empty or almost empty tunnels, whereas the dark spot in the middle of a ring of six black spots represents a more or less filled tunnel position. The HTB framework structure of corner-sharing WO_6 octahedra is shown in Fig. 1d. When all hexagonal tunnel sites are filled with lanthanum, the composition of the structure is $La_{0.33}WO_3$ ($x_{max} = 0.33$). Our recent thermal analysis and structural studies of the HTB-related La phase in argon and oxygen atmosphere showed that additional oxygen atoms are present in the structure, thus forming an almost fully oxidized compound of composition La_xWO_{3+y} with $x \approx 0.10$ (4). An RE content of $x \approx 0.10$ indicates that less than 40% of available RE positions are filled. In the superstructure of HTB-type, approximately 60% of the hexagonal tunnel sites are filled with RE^{3+} ions ($x \approx 0.20$). It thus seems likely that the superstructure is due to an ordered arrangement of RE^{3+}, oxygen ions and vacancies

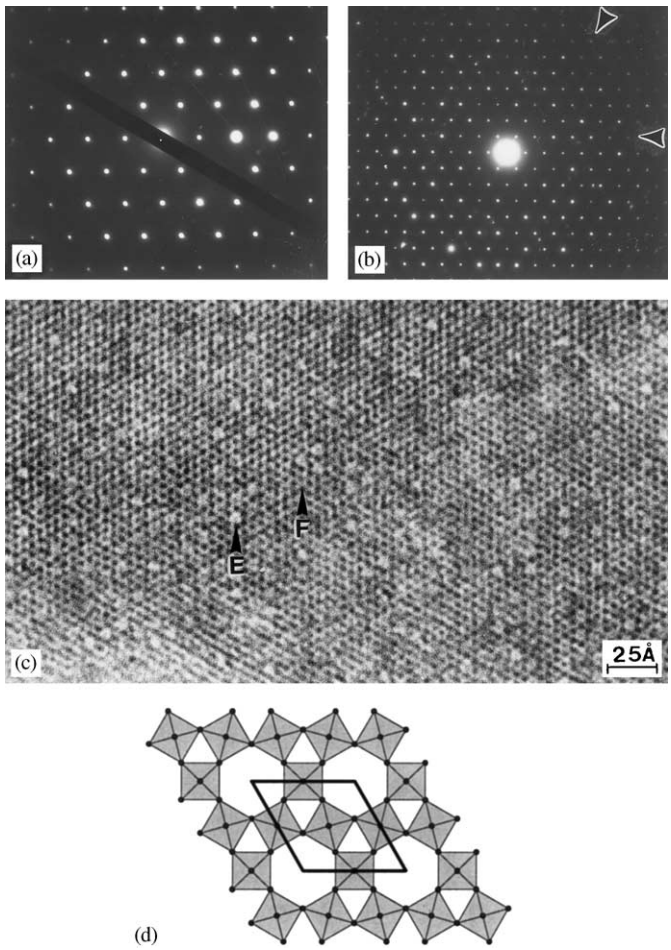

FIG. 1. Electron diffraction patterns of thin La_xWO_{3+y} crystals aligned along *c*. The La-content determined by EDS-analysis is (a) $x \approx 0.10$ and (b) $x \approx 0.20$. Two rows of superlattice reflections that double the *a*-axis parameter are marked by arrows in (b). (c) HRTEM image of a typical HTB-related crystal, $La_{0.10}WO_{3+y}$, with the corresponding ED pattern in (a). One empty or almost empty hexagonal tunnel is marked E, while F exemplifies a more or less filled tunnel position. (d) The basic framework structure of HTB in [001] projection. The La ions in the hexagonal tunnels are not shown. The unit cell is outlined.

in the hexagonal tunnels. It has not been possible to take HRTEM images of the superstructure, because these fragments are unstable and decompose to an amorphous phase under the imaging conditions in the JEOL 3010 electron microscope.

Our electron diffraction studies of the La- and Nd-containing samples established that high-pressure phases of (*n*)-ITB type ($n = 2$ and 3) can be prepared in the pressure region 25–30 kbar at $T > 1500$ K. The (3)-ITB phase could only be detected in the X-ray pattern of the sample prepared at the highest temperature, $T = 1620$ K. This is in agreement with the previous observation that higher temperature favours the formation of ITB phases with higher *n*-values (14). The EDS results in Tables 1 and 2 show a low *RE* content, $0.04 \leq x \leq 0.08$, for the (*n*)-ITB compounds, which indicates that $<40\%$ of the hexagonal tunnel sites in the ITB structures are filled with RE^{3+} ions. The value is lower for (3)-ITB than for (2)-ITB crystals, in agreement with the difference in x_{max}-values: 0.14 for (3)-ITB and 0.20 for (2)-ITB.

The HRTEM image in Fig. 2a ([001] zone) is taken of a (2)-ITB fragment from the $Nd_{0.10}WO_3$ sample, with the corresponding structure model shown in Fig. 2b. The (2)-ITB structure is built up of single hexagonal tunnel rows, and the WO_3 slabs are two octahedra wide ($n = 2$). A defect consisting of a double hexagonal tunnel row can be seen to the left in the image. It can be described as a slab of the (1,2)-ITB phase intergrown with the (2)-ITB structure. The HRTEM image also shows that there is a local

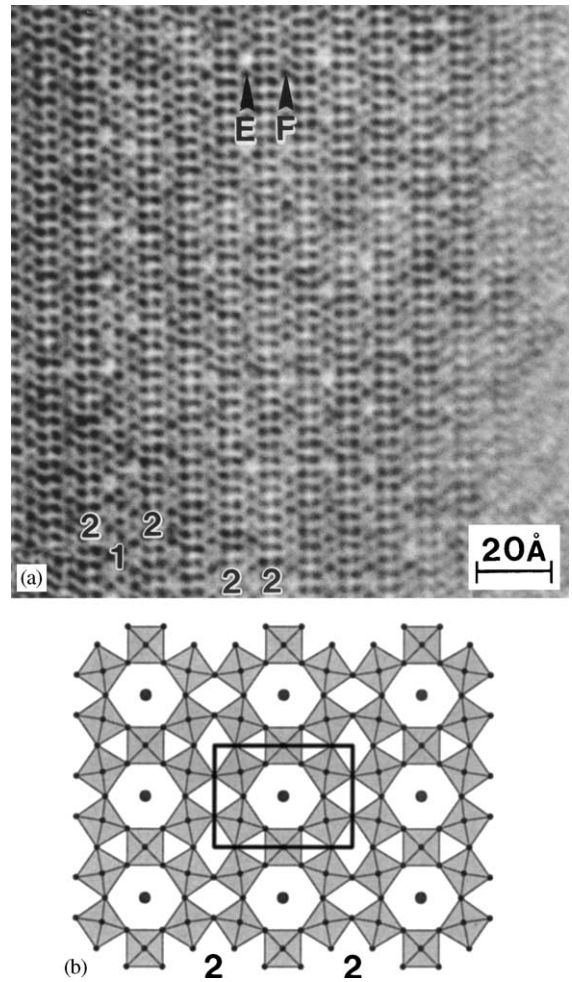

FIG. 2. (a) HRTEM image of an $Nd_{0.08}WO_{3+y}$ crystallite ([001]zone) and (b) the corresponding crystal structure of (2)-ITB with the unit- cell outlined. The dark dots in (b) represent the projected tunnel ions (Nd^{3+}). An isolated defect of (1, 2)-ITB-type is seen to the left. E denotes an empty or almost empty tunnel, and F shows a more or less filled one.

variation in the filling of the six-sided tunnels by the Nd ions. The larger white dots (marked E) indicate empty or almost empty hexagonal tunnels, and the black dots (marked F) show more or less filled ones. The HRTEM image in Fig. 2a does not show the location of the RE^{3+} ions along the *c*-axis. Such information might be obtained from an HRTEM image taken of a (2)-ITB crystal aligned along *b*, however. The micrograph in Fig. 3a with the corresponding ED-pattern inserted ([010] zone) is taken of a (2)-ITB crystal, La_xWO_{3+y} with $x \approx 0.08$. The ED pattern confirmed the unit cell dimensions given in Table 1. The *x* value indicates that about 40% of the hexagonal tunnel sites are filled by La ions. These ions are most likely located in the middle of the hexagonal tunnels, either in approximately the same plane as the tungsten atoms (Fig. 3b) or in the plane between the tungsten layers (Fig. 3c). The location of the La ions in the first model is similar to that recently observed for lanthanum in the HTB-related phase $La_{0.10}WO_{3+y}$, formed at high pressure. In the second model, the position of the La ion along *c* is analogous to that of alkali in the alkali intergrowth tungsten bronzes (15). Sets of theoretical images of the two structure models in Fig. 3b and 3c have been calculated for different defocus and crystal thickness values. A couple of these images are illustrated in Fig. 3d–3g. The results show that the contrast features in the HRTEM image agree well with the calculated image (Fig. 3d) of the structure model in Fig. 3b at a defocus value of –200 Å, which supports the hypothesis that the La ions are located in the same plane as the tungsten atoms. In analogy with the La-containing HTB-related phase described above, it also seems very likely that additional oxygen atoms are located in the hexagonal tunnels in the (2)-ITB structure, thus giving an almost fully oxidized compound of composition La_xWO_{3+y}.

RE_xWO_3 crystallites of PTB-type have been seen in most of the bulk samples with $x \leq 0.15$, prepared at $P \leq 50$ kbar. The ED/EDS studies of such fragments showed an *RE* content of $x = 0.08$–0.12, considerably less than the $x \leq 0.25$ value recently observed for RE_xWO_3 bronzes prepared under ambient pressure conditions (6). The ED patterns showed strong reflections typical of a cubic cell with $a \approx 3.8$ Å. Weak streaking and diffuse superlattice reflections in a twinned pattern (see Fig. 4) were seen in a few ED patterns taken along $\langle 110 \rangle$. The superlattice spots indicate a fairly ordered arrangement of RE^{3+}—in planes parallel to {111} in the PTB structure. The distances between these planes are in the range 12–13 Å, which is in agreement with those observed for the ambient-pressure RE_xWO_3 bronzes (6).

Isolated defects (see Fig. 2a) as well as disordered intergrowth arrangements of WO_3 slabs, two or three octahedra wide, and single or double hexagonal tunnel rows can be seen in a few crystals of (*n*)-ITB type. The ED

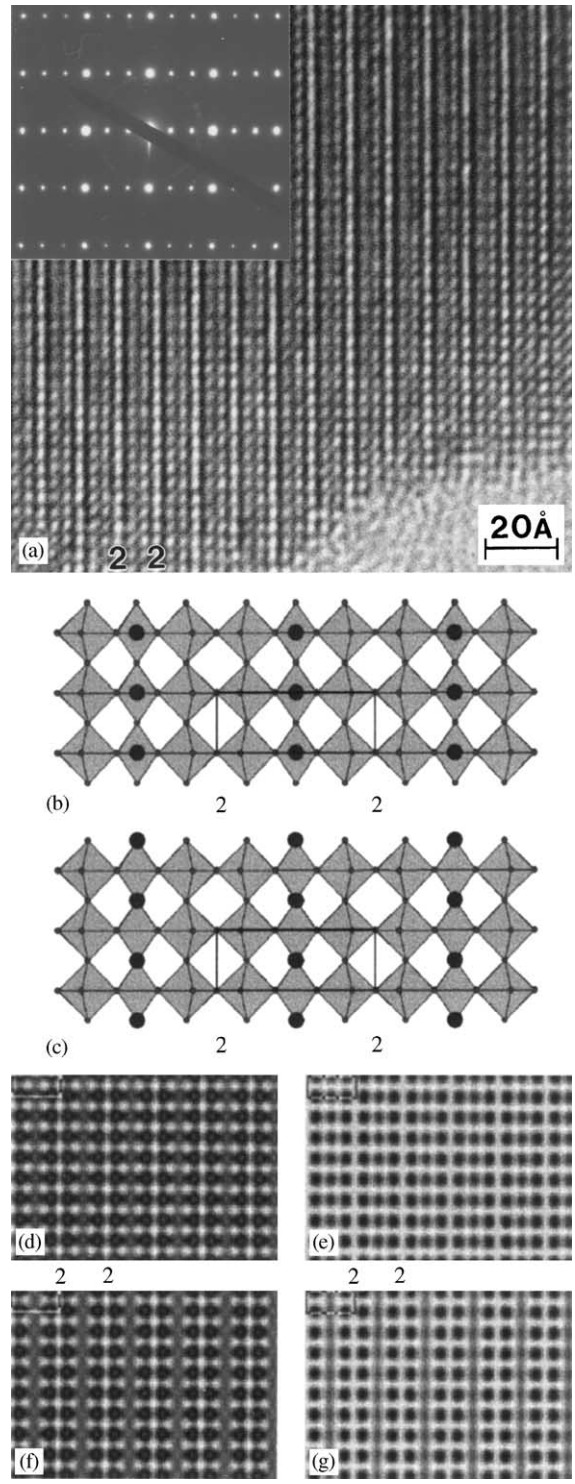

FIG. 3. (a) HRTEM image (with the corresponding ED-pattern inserted) of a (2)-ITB crystal in [010] projection. The corresponding structure models with the *RE* ions located in the same plane as the tungsten atoms (b) and in the plane between the tungsten layers (c). Simulated images of the structure model in (b) are illustrated in (d) and (e). Simulated images of the structure model in (c) are illustrated in (f) and (g). Crystal thickness ~30 Å, defocus values (d) –200 Å, (e) –300 Å, (f) –200 Å, and (g) –300 Å.

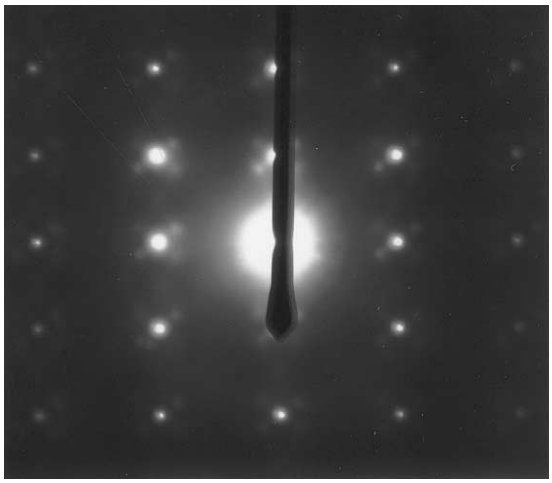

FIG. 4. ED pattern of an $La_{\sim 0.10}WO_3$ crystal aligned along $\langle 110 \rangle$ of the cubic unit cell with $a \approx 3.8$ Å. Streaking of the basic reflections and superlattice spots in twin orientations can be seen.

pattern in Fig. 5a is that of an Nd-containing (2)-ITB crystal in [001] projection. Streaking and additional weak reflections along a* indicate that there are disordered regions in the crystal structure. The corresponding HRTEM image in Fig. 5b shows intergrowth of isolated slabs of (1,3)-ITB and (3)-ITB in the (2)-ITB structure.

In addition to the tungsten-bronze-related phases RE_xWO_{3+y} with $0 \leq y \leq 3x/2$, the ED/EDS studies revealed a small amount of the high-pressure compound W_3O_8(II) (16), and some fragments of a so far unidentified phase with the ratio *RE*:W = 1:1, in most of the samples prepared at the highest pressure, $P = 80$ kbar. Fragments of the latter phase have also been seen in a few samples prepared at 50 kbar. From our ED/EDS and HRTEM studies, it seems very likely that the crystals with *RE*:W = 1:1 represent a new high-pressure phase. Further high-pressure syntheses and TEM studies of $REWO_x$ samples are in progress.

Thermal Stability of the HTB-Related RE_xWO_{3+y} Phases

Our recent thermal stability studies of the HTB-related La-containing phase showed that it is a metastable, almost fully oxidized compound of composition $La_xWO_{3+3x/2}$ with $x \approx 0.10$ (4). Further details about the phase transformation $RE_xWO_{3+3x/2}$ (HTB-related structure) → RE_xWO_3 (PTB-type structure) under ambient-pressure conditions were obtained by additional experiments on an $Nd_{0.20}WO_3$ sample consisting mainly of the HTB-related phase. Additional minor phases observed in the starting material were WO_3 and a compound with an *RE*:W ratio of 1:1. One part of the sample was heated in inert atmosphere to 1270 K, and other parts in evacuated silica tubes for different lengths time (see Table 3).

The X-ray powder patterns confirmed that the high-pressure phase, Nd_xWO_{3+y}, with an HTB-related structure is metastable at ambient pressure and is transformed into a PTB structure, Nd_xWO_3, with cubic symmetry, as can be seen in Fig. 6. The X-ray results in Table 3 show that the length of the *a*-axis in the HTB-structure increases from

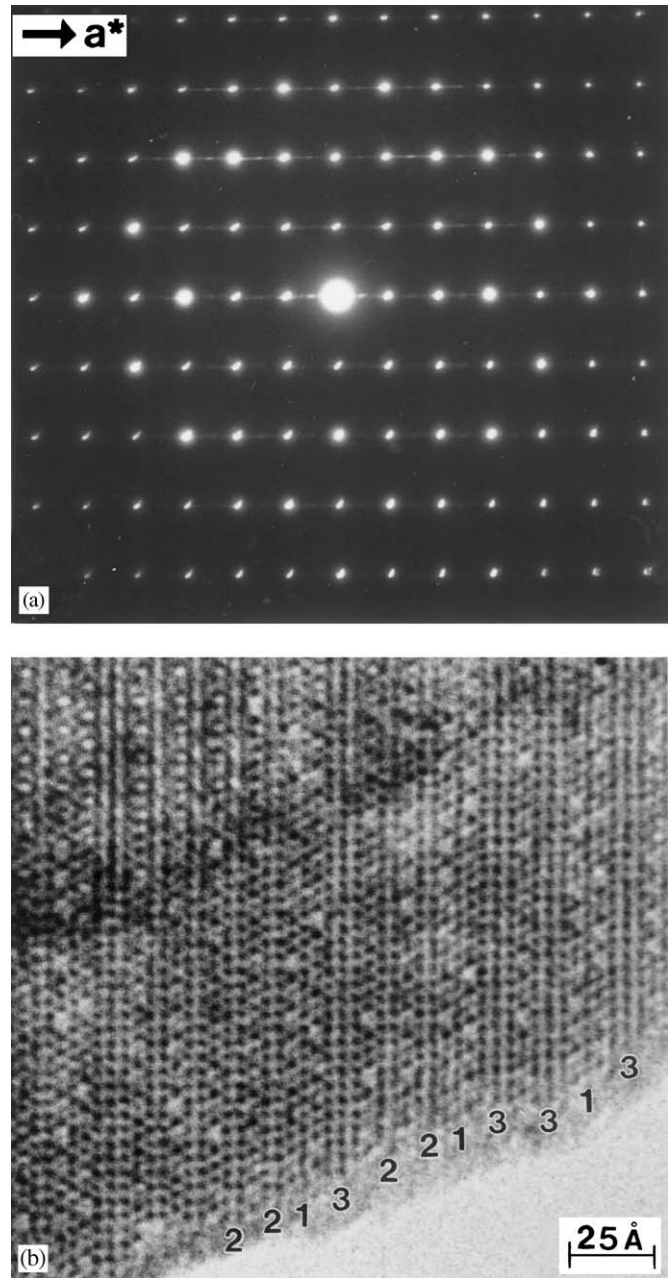

FIG. 5. (a) ED pattern taken from a disordered (2)-ITB crystal. Streaking and additional weak reflections can be seen along a*. The corresponding HRTEM image showing disordered intergrowth of isolated slabs of (1,3)-ITB and (3)-ITB in the (2)-ITB structure.

TABLE 3

Experimental Conditions and Unit-Cell Dimensions for the Phase Transition Nd_xWO_{3+y} (HTB-Related Structure) → Nd_xWO_3 (PTB Structure Type) Parts of the X-Ray Patterns (a)–(c) are Illustrated in Fig. 6

Starting material, Temp (K)	$Nd_{0.20}WO_3$ Time (h)	Phase	Unit cell dimensions a (Å)	c (Å)	V (Å^3)
(a) —	—	HTB	7.3911(2)	3.7914(2)	178.8
870	20	HTB	7.4065(6)	3.7920(4)	179.5
		PTB	3.8120(2)		55.39
(b) 870	70	HTB	7.4258(3)	3.7922(5)	180.5
		PTB	3.8205(1)		55.76
(c) 1270	TG treatment	PTB	3.8240(2)		55.92

7.3911 to 7.4258 Å, which means that the Nd–O distances increase from 2.688 to 2.701 Å. Table 3 also shows that the length of the a-axis in the PTB structure increases slightly during the heat treatment of the sample. The corresponding Nd–O distances are 2.695 and 2.704 Å. The Nd atom is 12-coordinated in the PTB structure and 7- or 8-coordinated in the HTB structure, as additional oxygen atoms are located in the hexagonal tunnels.

A few weak additional lines in the X-ray pattern of the final product could be identified as due to $Nd_2(WO_4)_3$ (see arrows in Fig. 6). The ED/EDS studies confirmed the presence of $Nd_2(WO_4)_3$ but, on the other hand, no crystals with an RE:W ratio of 1:1 could be found in the final product. In addition to the transformation of the tungsten-bronze related phases, the X-ray and ED/EDS-results seem thus to indicate that the unidentified compound with RE:W = 1:1 transforms into the neodymium tungstate $Nd_2(WO_4)_3$ during the heat treatment in argon atmosphere. The excess of Nd from this transformation process, probably reacts with the small amount of WO_3 seen in the bulk sample and form additional amounts of the $Nd_{\sim 0.1}WO_3$ (PTB-type) and $Nd_2(WO_4)_3$ phases.

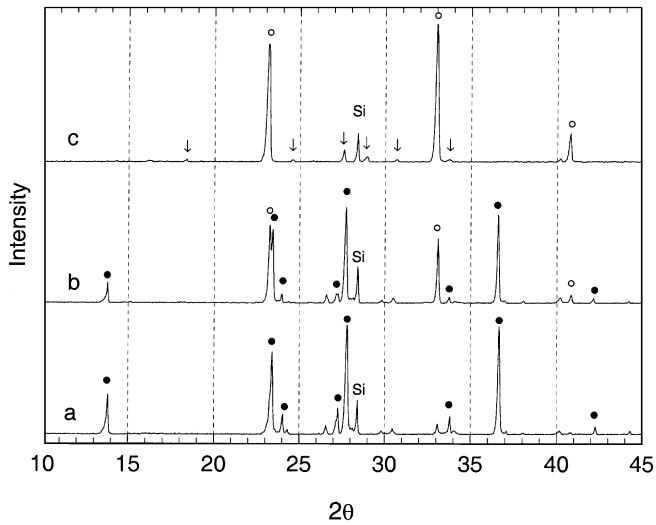

FIG. 6. Part of the X-ray patterns of $Nd_{0.2}WO_3$ heat-treated under different conditions. (a) Starting material; lines characteristic of the HTB phase are marked with black spots. (b) Heat-treated sample (in an evacuated Si-tube) at 870 K, 70 h. Lines characteristic of the HTB and PTB phases are marked with black spots and open circles, respectively. (c) Final product after TG treatment up to 1320 K. Open circles show lines of PTB, and arrows denote lines from $Nd_2(WO_4)_3$. No peaks of the HTB phase can be seen in the pattern.

PRESSURE–TEMPERATURE PHASE RELATIONS, AND DISCUSSION

The X-ray and electron microscopy results from the bulk samples, La_xWO_3 (Table 1) and Nd_xWO_3 (Table 2), show that three tungsten-bronze-related phases, HTB, ITB and PTB, were formed in the pressure–temperature range investigated. The results from the La- and Nd-containing samples are very similar in pressure–temperature–phase relations and RE content of the different crystal types. Our thermal stability studies of a few bulk samples showed that the PTB phases are reduced compounds of composition RE_xWO_3, whereas the HTB-related phases are probably fully oxidized materials of composition RE_xWO_{3+y} with $y \leq 3x/2$. The latter conclusion is also supported by the fact that in the bulk samples consisting mainly of HTB- and ITB-related phases, we have always observed small amounts of the reduced tungsten oxides W_3O_8(II) and WO_2. A tentative diagram of the pressure–temperature–phase relations for RE_xWO_{3+y} has thus been constructed and is shown in Fig. 7.

The HTB-related phases, which have been observed in all bulk samples prepared at $P \geq 20$ kbar, are located on a large field in the right-hand part of the P–T diagram. The PTB bronzes, on the other hand, are formed in the pressure region $P \leq 50$ kbar. The X-ray and ED/EDS results show that when the pressure is increased, the temperature must also be increased for the PTB bronzes to form. The PTB phases are thus located on the (upper) left-hand part of the diagram. The ITB-related phases are high-pressure, high-temperature phases, which seem to form in a small region at the boundary between the PTB and HTB compounds. The diagram shows that RE_xWO_{3+y}, with an HTB-related structure, is formed at constant pressure almost regardless of temperature, whereas RE_xWO_{3+y}, with an (n)-ITB-related structure and RE_xWO_3 with a PTB-type structure are the high-temperature phases. It is interesting to note that similar results have been obtained on alkali bronzes, A_xWO_3 (14), prepared under ambient-pressure conditions: the ITB bronzes were found to be high-temperature phases and the HTB bronzes low-temperature phases.

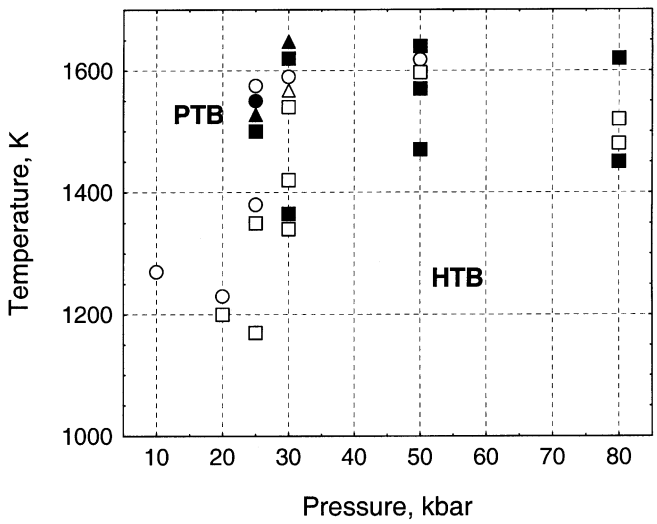

FIG. 7. Pressure–temperature (P–T) diagram showing the phase relationship for rare-earth tungsten-bronze-related phases, RE_xWO_{3+y} observed in the bulk samples La_xWO_3 (see Table 1) and $NdxWO_3$ (see Table 2). Unfilled symbols represent Nd phases, Filled symbols denote La phases. Squares represent HTB-related phases, triangles ITB-related phases, and circles PTB compounds.

In the present study, we have not observed any ITB-related phases in the RE_xWO_3 bulk samples prepared at 50 kbar. Such phases of (n)-ITB type were previously found in samples prepared in our first high-pressure experiments on the RE_2O_3–WO_3 systems with RE = Ce, Pr, Nd (1, 2). One reason for this difference might be that the starting compositions of the samples differ in oxygen content. The latter samples are fully oxidized starting materials. Another reason could be that the narrow temperature region (50–100 K) at the boundary between the HTB and PTB areas, in which the ITB phases seem to form, may have been missed during the synthesis experiments. This might be due to the temperature gradient in the high-pressure chamber, which has been estimated to be 30–50 K.

It is well known that pressure stabilizes higher-density phases. However, this rule is not true in the case of the tungsten-bronze-related phases, M_xWO_{3+y} with M = Ca, La, and Nd, which have PTB-type structures with $y = 0$ at ambient pressure conditions (7–9, 17), and HTB-related structures with $0 \le y \le 3x/2$ at high pressures [1–4, 18]. The former structure is denser than the latter one. This can be seen by comparing the values calculated by taking the volume of the unit cell divided by the number of oxygen atoms. This value is 18.6 Å^3 for $La_{0.09}WO_3$, PTB type, and 20.0 Å^3 for the HTB-type structure. The corresponding value for (2)-ITB is 19.0 Å^3, which is in between the two extremes. The P–T diagram in Fig. 7 shows that increasing pressure stabilizes the HTB-related structure. This phenomenon can be explained by considering the PTB structure (ABO_3) along the {111} directions where the oxygen and A-metal atoms form a cubic close packed (ccp) arrangement. This means that the size of the A ion (CN 12) should not exceed that of oxygen, r = 1.40 Å.This is true for Ca^{2+}, La^{3+} and Nd^{3+} ions, whose ionic radii are 1.34, 1.36, and 1.27 Å, respectively (19).

Structural studies of crystalline ReO_3-type WO_3 in the pressure region <50 kbar by Xu *et al.* (20) have recently shown that the unit cell has a rather high compressibility. The unit-cell volume of the high-pressure modification was observed to decrease by approximately 10% when the pressure was increased from 1.2 to 47.0 kbar. In analogy with these results, it thus seems likely that the voids in the PTB structure will decrease in size with increasing pressure, and that the size of Ca^{2+}, La^{3+}, and Nd^{3+} will become too large for the interstices in the WO_3 framework structure. This means that the stability border for the PTB structures will be slightly shifted towards ions with smaller ionic radius. For the ions listed above, the structure type will thus change from PTB to HTB or (n)-ITB, which contain hexagonal tunnels where the larger cations can be accommodated. The observed stability of the PTB-related phases under the pressure and temperature conditions shown in Fig. 7 can be explained by compensation of the unit-cell shrinkage due to pressure by thermal expansion with increasing temperature.

The RE content in the PTB- and HTB-related structures is always around $x \approx 0.1$ even if the bulk content is substantially higher. This means that less than 40% of the available RE positions in the hexagonal tunnels are occupied. However, it seems possible to synthesize at very high pressures ($P \ge 80$ kbar) RE_xWO_{3+y} compounds with HTB-related structures in which approximately $\frac{2}{3}$ of the available tunnel positions are occupied by La or Nd. Such crystals, observed in a few samples, were found to be fairly unstable under ambient-pressure conditions, and they decomposed due to heating in the electron beam of the microscope. The reason might be the high positive charge (3+) of the RE ions in the hexagonal tunnels. It is interesting to note that the situation is reversed for the alkali tungsten bronzes, A_xWO_3, which are formed for $0.19 \le x \le 0.33$, which means that more than 60% of the available hexagonal-tunnel positions are filled by alkali ions (A^{1+}) (21).

In view of the results obtained on the La- and Nd-containing samples above, it seems very likely that similar relationships between pressure, temperature and phase content would be obtained for all the larger RE ions (RE = La–Nd). For the smaller RE ions, on the other hand, other high-pressure RE-containing phases might form. Phase analysis studies of the WO_3–$RE_2W_2O_9$–W system with RE = Er–Lu have therefore been started in order to explore the effect of the RE ion size on the

formation of rare-earth tungsten oxides under high-pressure, high-temperature conditions.

ACKNOWLEDGMENTS

We wish to thank Jaroslava Östberg for technical assistance with the photographic work. The research described here was partly made possible by a Visiting Scientist Grant from the Royal Swedish Academy of Sciences through its Nobel Institute for Chemistry. This support is gratefully acknowledged. Financial support from the Swedish Natural Science Research Council and the Russian Foundation for Basic Research (Grant 01-03-32457) is also gratefully acknowledged.

REFERENCES

1. N. D. Zakharov, Z. Liliental-Weber, V. P. Filonenko, I. P. Zibrov, and M. Sundberg, *Mater. Res. Bull.* **31,** 373 (1996).
2. N. D. Zakharov, P. Werner, I. P. Zibrov, V. P. Filonenko, and M. Sundberg, *J. Solid State Chem.* **147,** 536 (1999).
3. C. Grenthe, M. Sundberg, V. P. Filonenko, and I. P. Zibrov, *J Solid State Chem.* **154,** 466 (2000).
4. V. P. Filonenko, C. Grenthe, M. Nygren, M. Sundberg, and I. P. Zibrov, *J Solid State Chem.* **163,** 84 (2002).
5. C. Grenthe, A. Guagliardi, M. Sundberg, and P.-E. Werner, *Acta Crystallogr. Sect. B* **57,** 13 (2001).
6. C. Grenthe and M. Sundberg, *J. Solid State Chem.* **167,** 412–419 (2002).
7. W. Ostertag, *Inorg. Chem.* **5,** 758 (1965).
8. I. N. Belyaev and L. A. Voropanova, *Russ. J. Inorg. Chem.* **21,** 1713 (1976).
9. P. J. Wiseman and P. G. Dickens, *J. Solid State Chem.* **17,** 91 (1976).
10. I. P. Zibrov, V. P. Filonenko, P.-E. Werner, B.-O. Marinder, and M. Sundberg, *J. Solid State Chem.* **141,** 205 (1998).
11. K.-E. Johansson, T. Palm, and P.-E. Werner, *J. Phys. E* **13,** 1289 (1980).
12. P.-E. Werner, *Ark Kemi* **31,** 513 (1969).
13. M. A. O'Keefe, P. R. Buseck, and S. Iijima, *Nature* (London) **274,** 322 (1978).
14. A. Hussain, *Chem. Commun. Univ. Stockholm* **2,** 1 (1978).
15. A. Hussain, *Chem. Scr.* **11,** 224 (1977).
16. M. Sundberg, N. D. Zakharov, I. P. Zibrov, A. Barabanenkov, V. P. Filonenko, and P. Werner, *Acta Crystallogr. Sect. B* **49,** 951 (1993).
17. D. Vandeven, J. Galy, M. Pouchard, and P. Hagenmuller, *Mater. Res. Bull.* **2,** 809 (1967).
18. N. D. Zakharov, P. Werner, I. P. Zibrov, V. P. Filonenko, and M. Sundberg, *Cryst. Res. Technol.* **35,** 713 (2000).
19. R. D. Shannon, *Acta Crystallogr. Sect. A* **32,** 751 (1976).
20. Y. Xu, S. Carlson, and R. Norrestam, *J. Solid State Chem.* **132,** 123 (1997).
21. A. Hussain, *Acta Chem. Scand. A* **32,** 479 (1978).